

Hashing-based Non-Maximum Suppression for Crowded Object Detection

Jianfeng Wang, Xi Yin, Lijuan Wang, Lei Zhang

Microsoft

{jianfw, xiyin1, lijuanw, leizhang}@microsoft.com

Abstract. In this paper, we propose an algorithm, named hashing-based non-maximum suppression (HNMS) to efficiently suppress the non-maximum boxes for object detection. Non-maximum suppression (NMS) is an essential component to suppress the boxes at closely located locations with similar shapes. The time cost tends to be huge when the number of boxes becomes large, especially for crowded scenes. The basic idea of HNMS is to firstly map each box to a discrete code (hash cell) and then remove the boxes with lower confidences if they are in the same cell. Considering the intersection-over-union (IoU) as the metric, we propose a simple yet effective hashing algorithm, named IoUHash, which guarantees that the boxes within the same cell are close enough by a lower IoU bound. For two-stage detectors, we replace NMS in region proposal network with HNMS, and observe significant speed-up with comparable accuracy. For one-stage detectors, HNMS is used as a pre-filter to speed up the suppression with a large margin. Extensive experiments are conducted on CARPK, SKU-110K, CrowdHuman datasets to demonstrate the efficiency and effectiveness of HNMS. Code is released at <https://github.com/microsoft/hnms.git>.

1 Introduction

Recent years have seen a great progress on object detection based on deep convolutional neural networks. The approaches can be roughly categorized as two-stage detectors [16,10] and one-stage detectors [15,14,11]. In two-stage detectors, a region proposal network (RPN) [16] is designed to propose candidate bounding boxes, which are used by the detection head network to refine the bounding box coordinates and to predict the classification scores. The one-stage detector directly predicts the box coordinates and classification result in one network pass. As one of the most essential post-processing steps, non-maximum suppression (NMS) is used to remove the boxes with similar locations and shapes but lower confidences.

Different variants of NMS have been proposed to improve the detection accuracy [1,7,13,6]. Instead of discarding the boxes, soft NMS [1] decays the confidence score as a continuous function of the intersection-over-union (IoU) and keeps all the boxes. While the continuous function is manually designed in [1], a special network is learned in [7] to rescore the confidence. Beyond altering

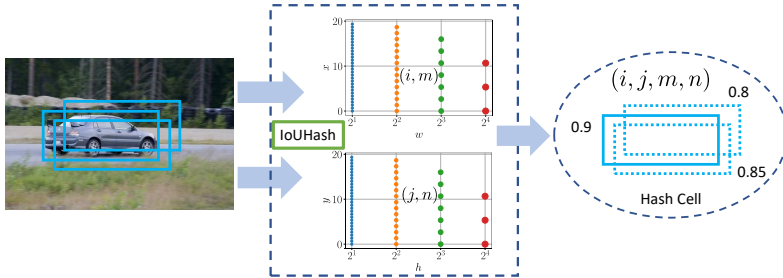


Fig. 1: Illustration of Hashing-based NMS process. Each bounding box is hashed to four index numbers by the proposed IoUHash function. The box width and height are hashed as $(i, j) \in \mathbb{Z}^2$ based on log scale and the offset is hashed as $(m, n) \in \mathbb{Z}^2$. The dots in the figure means the center of the hash cell. In each hash cell, the box (in solid line) with highest confidence score is kept, and all others (in dotted line) are suppressed. A lower bound can be derived to guarantee the closeness between any two boxes within the same cell.

the confidence, the bounding box coordinates are also updated in [13,6] during suppressing neighboring boxes to improve the location accuracy.

For the time cost, the NMS complexity in the worst case is $O(N^2)$, where N is the number of boxes. Thus, the time cost becomes remarkably high when the number of boxes is large. This problem is more severe in object detection with crowded scene as thousands of boxes are generated in RPN for NMS.

To improve inference speed, [2] proposed MaxPoolNMS to replace the NMS in RPN by a max pooling operation over the objectness. It implicitly assumes that boxes from nearby anchor boxes are also similar. However, this assumption cannot be guaranteed theoretically because the bounding box regression could change the box coordinates dramatically without any constraint.

To reduce the time cost and address the issues in existing approaches, we propose a hashing-based NMS (HNMS) approach, which has $O(N)$ time complexity. As illustrated in Fig. 1, the basic idea is to map each box location into a discrete hash value. Traditionally, a hash function maps different box locations to different values even if the boxes are close to each other. Instead, we expect that the boxes at neighboring locations and with similar shapes are mapped to the same hash value, and the boxes located far away should be mapped to different hash values. The region where different boxes are hashed to the same value is denoted as a *hash cell*. In this way, we can remove the boxes with lower confidence within each cell. The idea is similar to the hashing-based nearest neighbor search (NNS) problem [9,3,21,19,18,20], where similar points are expected to be mapped to similar hashing values. In NNS, the metric is normally based on Euclidean distance, and thus the designed function is inappropriate for the detection problem because of the IoU metric. For example, two bounding boxes can have small difference in Euclidean distance, but can be far away from each other in IoU.

Considering the definition of IoU, we propose a simple yet effective hashing function, named IoUHash. The design principle is to make it simple and make the size of each hash cell as similar as possible. Given two boxes with the constant IoU, if the size is larger, the offset difference can be farther. Thus, we hash the size first (in logarithmic scale) and then the offset (in natural scale) based on the size. Analytically, we can derive a lower IoU bound regardless of the cell index if two boxes are within the same hash cell, which guarantees the suppressed boxes are close enough to the box with highest confidence.

One issue is that two boxes may be located in adjacent cells and near the boundary. In this case, both boxes may not be suppressed though their actual IoU is large. To address this issue, we apply the HNMS multiple times with different IoUHash functions, where the cell partition parameters are different. For two-stage detectors, we directly replace NMS by our HNMS in RPN, and observe no accuracy loss but significant speed gain for the suppression module, e.g. 7.4x on CARPK in CPU mode. For one-stage detector, we apply HNMS as a pre-filtering step which greatly reduces the number of boxes to be filtered by NMS and the overall time cost, e.g. resulting in 6.8x speed up on CARPK in GPU mode.

2 Preliminary

To make the paper self-contained, we first review the problem that NMS tries to solve and then describe the details of NMS.

2.1 Problem Description

Let N be the number of bounding boxes and $\mathbf{B} \in \mathbb{R}^{N \times 4}$ be the coordinate matrix, where each row corresponds to the location of each box. Normally, each box can be described by its box size $\{w, h\}$ and center point offset $\{x, y\}$ or its top-left and bottom-right corners $\{x_{left}, y_{top}, x_{right}, y_{bottom}\}$. In this paper, we will use the center offset and size representation $\{w, h, x, y\}$ to describe our algorithm and use *offset* to denote center point offset for simplicity. A confidence score $s \in [0, 1]$ is attached to every box to indicate the likelihood belonging to the specific class or the general object (e.g. RPN). Let $\mathbf{s} \in [0, 1]^N$ be the corresponding confidence vector. The problem is that multiple boxes with similar shapes may be located for a single object, and we need to keep one and suppress the others.

2.2 Non-Maximum Suppression

The algorithm of NMS can be described as follows. All boxes are initialized as *unsuppressed*. Then, it goes through each unsuppressed box in a descending order of the confidence score. IoU is calculated between the current box (with higher confidence) and all the unsuppressed boxes with lower confidences. The boxes with IoU larger than a pre-defined threshold are suppressed. This process will continue until all boxes are checked.

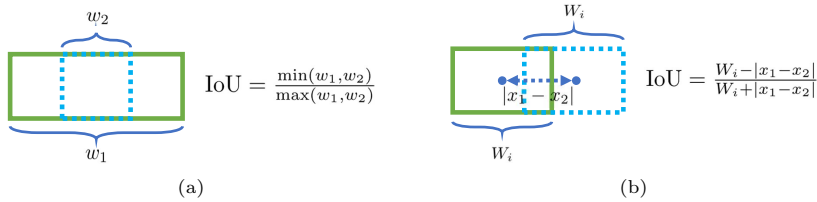


Fig. 2: IoU calculation for deriving IoUHash.

The sorting takes $O(N \log(N))$ time complexity. If each unsuppressed box can suppress S boxes on average, the time complexity of the two loops is $O(N^2/(S+1))$. In the worst case where no box is suppressed, the complexity is $O(N^2)$. If all the other boxes are suppressed by the first box (highest confidence score), the time complexity is $O(N)$. Thus, the time cost ranges from $O(N \log(N)) + O(N)$ to $O(N \log(N)) + O(N^2)$. Next, we will present our proposed approach which has $O(N)$ time complexity independent of the data distribution.

3 Proposed Approach

The core idea is to quantize the continuous-valued box coordinates to discrete values and then perform non-maximum suppression within each hash cell. Thus, we first introduce the hashing function in Sec. 3.1 and then the suppression logic in Sec. 3.2. Sec. 3.3 gives a discussion on the performance.

3.1 IoUHash Function

To make it simple, we design the function to be data-independent, i.e. no parameters are required to learn from the data. Another principle is to make the expected IoU roughly the same if any two boxes are hashed to the same cell. In this way, all hash cells can be treated equally.

Based on the IoU definition, if the widths and heights of two boxes are both larger, their offsets can be farther to have the same IoU. If two boxes are both small, a slight offset change would lead to large IoU change. To make the IoU the same, the offset quantization should be based on the box size. Thus, we propose to quantize the size first and then the offset.

The width and height are quantized independently for simplicity. Take the width as an example. If two boxes are of the same height and offsets, their IoU can be written as $\min(w_1, w_2) / \max(w_1, w_2)$, where w_1 and w_2 are the widths of the boxes, as illustrated in Fig. 8 (a). This motivates us to design the function such that 1) the width is partitioned into multiple disjoint ranges, and 2) the ratio of the range centers should be the same if we attach a center point to each range. Let $\{W_i, i \in \mathbb{Z}\}$ be the range centers. That is, we should have $\alpha \triangleq W_i/W_{i+1}, \forall i$, where α is the pre-defined parameter, or

$$W_i = W_0/\alpha^i, i \in \mathbb{Z}, \quad (1)$$

where W_0 is the 0-th cell center as a parameter. Note that the index of i can be smaller than 0. With a log operation, we have $\log(W_i) = \log(W_0) - i \log(\alpha_w)$. In other words, the width is equally partitioned in the log-scale. Given any box with width w , we quantize the width as the i -th cell if

$$i = \lfloor (\log(W_0) - \log(w)) / \log(\alpha) \rfloor, \quad (2)$$

where $\lfloor \cdot \rfloor$ means the integer round operation. With this design, if two boxes are of the same height and offset, and with widths being two adjacent range centers (e.g. W_i and W_{i+1}), their IoU is always α for any i . If their widths also falls into the same range (e.g. W_i), the minimum IoU is also α . Thus, α represents the distance between adjacent cells and the cell size. Similarly, the height h is quantized to the j -th cell if

$$j = \lfloor (\log(H_0) - \log(h)) / \log(\alpha) \rfloor, \quad (3)$$

where H_0 is the 0-th cell for the height.

After quantizing the width and height, we also hash the x -offset and y -offset independently. Take the x -offset for instance. Given two boxes, assume that the widths are identical and equal to W_i (Eqn. 1), the heights and y -offsets are also the same, but x -offsets (x_1 and x_2) are different. Then, the IoU is $(W_i - |x_1 - x_2|) / (W_i + |x_1 - x_2|)$, shown in Fig. 8 (b) if $|x_1 - x_2| \leq W_i$, and 0, otherwise. As we can see, the IoU is only related to the distance between the centers in the x direction in this case. This leads us to quantize the x -axis equally. Let X_m be the partition center, and $\delta_i \triangleq X_{m+1} - X_m$ be the distance between any two adjacent partition centers. Note, the δ_i depends on W_i , which represents how wide the box is. If two boxes falls into two adjacent partition centers, their IoU is designed to be α (recall that α represents the distance of the adjacent width/height cells), i.e. $\alpha = (W_i - \delta_i) / (W_i + \delta_i)$. Then, we have

$$\delta_i = W_i(1 - \alpha) / (1 + \alpha) \quad (4)$$

$$X_m = b_x \delta_i + m \delta_i, m \in \mathbb{Z} \quad (5)$$

where b_x is a parameter. Given the horizontal offset as x , we hash it to

$$m = \lfloor x / \delta_i - b_x \rfloor. \quad (6)$$

Similarly, the vertical offset y is quantized as

$$n = \lfloor y / \delta_j - b_y \rfloor, \quad (7)$$

where

$$\delta_j = H_j(1 - \alpha) / (1 + \alpha), \quad (8)$$

$$H_j = H_0 / \alpha^j. \quad (9)$$

The algorithm is described in Alg. 1. In summary, given any two boxes, if any three dimensions (e.g. width, height, x -offset) are the same and equal to the corresponding cell center, and the other dimension are equal to the adjacent cell centers, the IoU is always α . If the unequal dimension is also hashed to the same cell, the minimum IoU is also always α .

Algorithm 1 IoUHash**Input:** Bounding box (w, h, x, y) , and hyper-parameters $W_0, H_0, b_x, b_y, \alpha$ **Output:** Hash code (i, j, m, n)

- 1: Calculate i based on Eqn. 2 with W_0 and α
- 2: Calculate j based on Eqn. 3 with H_0 and α
- 3: Calculate W_i based on Eqn 1 with W_0 and i
- 4: Calculate H_j based on Eqn 9 with H_0 and j
- 5: Calculate δ_i based on Eqn 4 with W_i and α
- 6: Calculate δ_j based on Eqn 8 with H_j and α
- 7: Calculate m based on Eqn. 6 with x, δ_i and b_x
- 8: Calculate n based on Eqn. 7 with y, δ_j and b_y
- 9: return (i, j, m, n)

Relation with Related Work This idea of quantizing the box is similar to the anchor size design in the detection framework, e.g. in FPN [10], Faster R-CNN [16]. Each ground truth box is assigned to different anchors during training, which is analogous to the process of hashing each box to different cells. One major difference is that the anchor sizes are designed jointly. For example in Faster R-CNN[16], the aspect ratio of width and height is set to be $1 : 1, 2 : 1$ or $1 : 2$. Comparably, we design the width and height independently. If each component has Q different cells, we can have as many as Q^2 different *anchors*, which is normally much larger than the number of anchor shapes.

MaxPoolNMS [2] performs the suppression by a max pooling over the objectness in RPN. If we treat anchors as hash cells, the approach can be interpreted as hashing each proposal to its corresponding anchor and suppressing other boxes in adjacent cells. The quantization here implicitly ignores the bounding box regression, which can change the box location without any constraint. Comparably, we perform hashing on regressed boxes to make each cell more compact. Another difference is that we suppress boxes within the same cell rather than in adjacent cells.

IoU Upper and Lower Bound If two bounding boxes are mapped to the same cell, the upper IoU bound is 1 if the two boxes are identical. Next, we calculate the lower bound.

Let (w_1, h_1, x_1, y_1) and (w_2, h_2, x_2, y_2) be two boxes, which are quantized to the same cell. Then, the intersection area can be written as $I = F(r - l)F(b - t)$, where $F(x) = x$ if $x > 0$ and 0, otherwise; and

$$l = \max(x_1 - \frac{1}{2}w_1, x_2 - \frac{1}{2}w_2), r = \min(x_1 + \frac{1}{2}w_1, x_2 + \frac{1}{2}w_2) \quad (10)$$

$$t = \max(y_1 - \frac{1}{2}h_1, y_2 - \frac{1}{2}h_2), b = \min(y_1 + \frac{1}{2}h_1, y_2 + \frac{1}{2}h_2). \quad (11)$$

If their centers are far enough, their intersection can vanish to 0 and the smallest IoU is 0. To avoid such cases, we should have the following condition (omitting

the requirement on y_1, y_2) hold always:

$$x_1 + \frac{1}{2}w_1 > x_2 - \frac{1}{2}w_2, x_2 + \frac{1}{2}w_2 > x_1 - \frac{1}{2}w_1, \quad (12)$$

which is equivalent to

$$|x_1 - x_2| < \frac{1}{2}(w_1 + w_2). \quad (13)$$

Since the two boxes are in the same cell, the largest value of $|x_1 - x_2|$ is equal to δ_i if they fall into the i -th width cell according to Eqn. 2. The smallest value of w_1 (or w_2) is $\alpha^{0.5}W_i$, which is the boundary between W_{i-1} and W_i . Thus, if we have the following condition hold

$$(1 - \alpha)/(1 + \alpha) < \alpha^{0.5}, \quad (14)$$

their IoU is always larger than 0. With $\alpha = 0.3$, Eqn. 14 holds. When α is increased, the right side is larger but the left side is smaller, which means the requirement is always satisfied when $\alpha \geq 0.3$. Next, we derive the lower bound under this condition.

Due to the same cell the two boxes are quantized into, we can express each component by the distance to the cell center as

$$\begin{aligned} w_k &= W_0/\alpha^{i+i_k}, & i_k &\in [-0.5, 0.5] \\ h_k &= H_0/\alpha^{j+j_k}, & j_k &\in [-0.5, 0.5] \\ x_k &= b_x\delta_i + (m + m_k)\delta_i, & m_k &\in [-0.5, 0.5] \\ y_k &= b_y\delta_j + (n + n_k)\delta_j, & n_k &\in [-0.5, 0.5] \end{aligned} \quad (15)$$

where $k = 1, 2$, i, j, m, n is the hash code for each dimension. By substituting Eqn. 15 to the IoU definition, we can easily conclude that the IoU has no relation with $b_x, b_y, W_0, H_0, i, j, m, n$, but only depends on α , and i_k, j_k, m_k and n_k , which are all bounded from -0.5 to 0.5. Meanwhile, we can see that the minimum IoU must reside in one of the boundaries, where i_k, j_k, m_k , and n_k equals -0.5 or 0.5. Instead of sticking to a closed form of lower bound, we calculate the lower bound by 1) selecting any $b_x, b_y, W_0, H_0, i, j, m, n$ since the IoU is constant with these values, 2) enumerating all the combinations of different i_k, j_k, m_k and n_k (equal -0.5 or 0.5), which means 2^8 different combinations for two boxes, 3) calculating the bounding box coordinates by Eqn. 15 for each combination; 4) calculating the IoU and choosing the minimum IoU, which is the lower bound. The algorithm flow and more details can be found in Appendix A.

Fig. 3 shows the lower IoU bound with different α . As we can see, the bound is a monotone non-decreasing function of α . When $\alpha = 0.3$, the bound is $1.4e^{-4}$, and thus if $\alpha \geq 0.3$, the IoU between any two boxes within the same hash cell is guaranteed to be larger than 0. This conclusion is consistent with satisfying Eqn. 14.

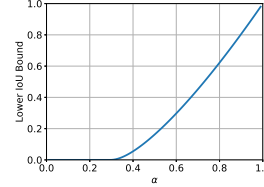


Fig. 3: Lower IoU bound as a function of α .

Algorithm 2 Hashing-based Non-Maximum Suppression

Input: Bounding box $\mathbf{B} \in \mathbb{R}^{N \times 4}$, confidence score $\mathbf{s} \in [0., 1.]^N$, $\alpha, b_x, b_y, W_0, H_0$ **Output:** Indices of kept boxes

```

1:  $\mathbf{C} = \text{IoUHash}(\mathbf{B})$  (Alg. 1) with  $\alpha, W_0, H_0, b_x, b_y$ 
2:  $\text{code2idx} = \{\}$ 
3: for  $i$  in  $[0, N - 1]$  do
4:   if  $\mathbf{C}_i$  in  $\text{code2idx}$  then
5:      $\text{pre} = \text{code2idx}[\mathbf{C}_i]$ 
6:     if  $s[\text{pre}] < s[i]$  then
7:        $\text{code2idx}[\mathbf{C}_i] = i$ 
8:     end if
9:   else
10:     $\text{code2idx}[\mathbf{C}_i] = i$ 
11:   end if
12: end for
13: return  $\text{code2idx.values}()$ 

```

3.2 Hashing-based Non-Maximum Suppression

After mapping each box to a hash cell by IoUHash, we simply keep the box with the largest confidence score and remove all others within each cell. The process can be described in Alg. 2.

Though we have a lower bound to guarantee the lowest IoU between any two boxes within the same cell, it cannot guarantee any two boxes with IoU larger than the lower bound falls to the same cell. For example, two boxes are close enough and have high IoU, but they can be hashed into two adjacent hash cells though they are very close to the boundary of the two adjacent cells. To solve the problem, we apply HNMS processes multiple times with different parameters. In IoUHash, α controls the size of each cell, while W_0, H_0, b_x, b_y controls the offset. Given α , we equally split the space to generate multiple IoUHash functions. Let K be the number of IoUHash functions. The k -th ($k \in [0, K-1]$) IoUHash's parameters ($W_0^{(k)}, H_0^{(k)}, b_x^{(k)}, b_y^{(k)}$) is calculated by satisfying the following condition,

$$\begin{aligned} \log(W_0^{(k)}) &= -\log(\alpha)k/K, \log(H_0^{(k)}) = -\log(\alpha)k/K \\ b_x^{(k)} &= k/K, \quad b_y^{(k)} = k/K. \end{aligned} \quad (16)$$

That is, $\log(W_0^{(k)})$ equally splits the range from $\log(1)$ to $\log(1) + (-\log(\alpha))$, and $b_x^{(k)}$ equally splits the range from 0 to 1. The whole process with multi HNMS is illustrated in Alg. 3.

3.3 Discussion

Approximation. Obviously, the complexity of HNMS is $O(N)$, which is faster than the vanilla NMS ($O(N \log(N) + O(N^2/(S+1)))$). If all boxes are split into

Algorithm 3 Multi HNMS

Input: Bounding box $\mathbf{B} \in \mathbb{R}^{N \times 4}$, confidence score $\mathbf{s} \in [0., 1.]^N$, K , α .

Output: Indices of kept boxes

- 1: Init an empty array of HNMS with length K
- 2: **for** k in $[0, K - 1]$ **do**
- 3: Calculate $(W_0^{(i)}, H_0^{(i)}, b_x^{(i)}, b_y^{(i)})$ based on Eqn. 16
- 4: HNMS[i] = IoUHash with the parameter of $W_0^{(i)}$
- 5: **end for**
- 6: keep=[1: N - 1]
- 7: **for** i in $[0, K - 1]$ **do**
- 8: currkeep = HNMS[i](\mathbf{B} , \mathbf{s}) based on Alg. 2
- 9: keep = keep[currkeep]; $\mathbf{B} = \mathbf{B}$ [currkeep]; $\mathbf{s} = \mathbf{s}$ [currkeep]
- 10: **end for**
- 11: return keep

positive boxes and negative boxes based on the NMS filter result, HNMS can be regarded as an approximate process of NMS, and has the following misaligned cases.

First, if the lower bound is lower than the NMS threshold, within each cell, HNMS could suppress the boxes with lower IoU, which leads to lower recalls. For this problem, we need a smaller hash cell or a higher α . Second, if the lower bound is higher than threshold, HNMS may fail to suppress the boxes whose IoU is larger than the threshold. This can lead to false positives or lower precision. For this problem, we need a larger hash cell or lower α . Third, if the lower bound is exactly the same as the threshold, HNMS might still fail to suppress some negative boxes or fail to keep some positive boxes. The reason is that NMS always suppresses boxes by unsuppressed boxes, while HNMS suppresses boxes within each cell and the box with the highest confidence might be a suppressed box in NMS. For example, we have three boxes A (100, 100, 54.1, 50), B (100, 100, 79.1, 50), C (100, 100, 96.1, 50). The four numbers are width, height, center x -offset and center y -offset. The confidence scores are 0.9, 0.8, 0.7, respectively. For HNMS, $W_0 = H_0 = 1$, $b_x = b_y = 0$, $\alpha = 0.73$. The lower IoU bound is 0.5015, which is set as the NMS threshold. The IoU between A and B is 0.7100, and thus B is suppressed. The IoU between A and C is 0.4934, and is lower than the threshold. Thus, the result is A and C. Based on Alg. 2, the result is A and B because B and C are in the same cell. Thus, C is missed and B is kept.

Since HNMS is not exactly equivalent to NMS, we apply HNMS in the following way. In two-stage detectors, we directly replace NMS in RPN by HNMS and observe significant speed up without any accuracy loss. The reason is that the RoI head is able to fix imperfect proposals. NMS in the RoI head is not changed since we find the time cost of NMS is minor. In one-stage detectors, we insert the HNMS as a pre-filter before applying the NMS, which greatly reduces the number of boxes for NMS and the overall (HNMS + NMS) time cost can also be reduced significantly.

Table 1: Experimental results with Faster-RCNN-R50-FPN. RPN-NMS and Total represent the time cost in ms. Speed is relative to RPN-NMS.

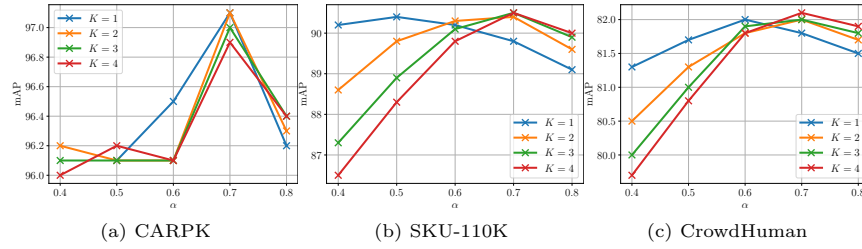
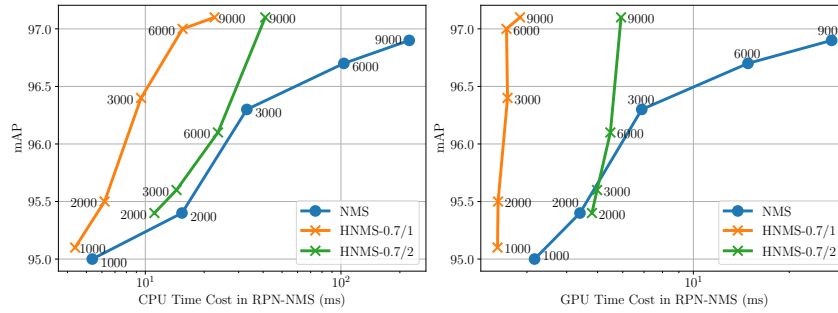
(a) CARPK									
		CPU			GPU				
	K	mAP	RPN-NMS	Speed	Total	RPN-NMS	Speed	Total	
NMS		96.9	223.3 ± 36.5	1x	3935.7	27.2 ± 2.0	1x	149.0	
HNMS	1	97.1	30.3 ± 5.4	7.4x	3665.6	6.5 ± 1.0	4.2x	132.8	
	2	97.1	49.0 ± 6.5	4.6x	3571.5	9.3 ± 1.2	2.9x	137.9	
	3	97.0	52.3 ± 7.6	4.3x	3790.5	11.2 ± 1.5	2.4x	136.9	
	4	96.9	68.8 ± 9.6	3.2x	3790.6	13.2 ± 1.7	2.1x	136.2	
(b) SKU-110K									
		CPU			GPU				
	K	mAP	RPN-NMS	Speed	Total	RPN-NMS	Speed	Total	
NMS		90.5	478.4 ± 64.4	1x	2599.9	32.2 ± 3.7	1x	133.7	
HNMS	1	89.8	41.4 ± 5.8	11.6x	2191.5	5.9 ± 0.6	5.5x	101.4	
	2	90.4	69.2 ± 7.4	6.9x	2220.2	8.6 ± 0.6	3.7x	103.8	
	3	90.5	79.9 ± 11.8	6.0x	2250.3	11.4 ± 1.3	2.8x	107.8	
	4	90.5	102.6 ± 11.8	4.7x	2239.9	17.1 ± 1.9	1.9x	101.4	
(c) CrowdHuman									
		CPU			GPU				
	K	mAP	RPN-NMS	Speed	Total	RPN-NMS	Speed	Total	
NMS		82.1	307.9 ± 48.4	1x	3643.5	27.3 ± 4.3	1x	148.8	
HNMS	1	81.8	38.9 ± 6.6	7.9x	3379.8	6.3 ± 0.8	4.3x	101.8	
	2	82.0	53.8 ± 6.7	5.7x	3584.5	10.4 ± 1.3	2.6x	114.4	
	3	82.0	64.1 ± 9.4	4.8x	3530.9	12.6 ± 0.8	2.2x	110.6	
	4	82.1	73.0 ± 10.9	4.2x	3434.4	15.4 ± 0.9	1.8x	113.7	

Implementation. Based on Sec. 3.1 and Sec. 3.2, we can easily implement the CPU code. For GPU, the challenging part is the suppression logic since different hash cells can have different numbers of boxes. For this problem, we implement it in the following way. First, we convert each hash code (i, j, m, n) to a unique integer. Second, we find the unique hash code and the index of the unique hash code based on the integer. Third, we calculate the maximum confidence score for each unique code by the atomic max operation. Finally, we find the index of the box with maximum score by the atomic compare-and-swap operation. Further details can be found in Appendix B.

4 Experiment

4.1 Settings

We conduct experiments on three datasets: CARPK [8], SKU-110K [5], and CrowdHuman [17]. CARPK is a car parking lot dataset, which contains 989 training images with 43 boxes/image and 459 test images with 103 boxes/image. SKU-110K was collected in retail environment for product item detection, which provides 8.2K training images with 147 boxes per image and 2,941 testing


 Fig. 4: Accuracy with different α and K for HNMS with Faster-RCNN-R50-FPN.

 Fig. 5: Accuracy vs time cost with different maximum numbers (shown in the figure) of boxes for filtering with Faster-RCNN-R50-FPN on CARPK for CPU and GPU. Our approach is denoted as HNMS- α/K .

images with 147 boxes/image. CrowdHuman is a benchmark dataset for crowded person detection, which has 15K training images with 29 boxes/image and 4,730 validation images with 27 boxes/image. It provides visible person box, full body box and human head annotations. Here, we use the visible person box annotation. The region marked as *mask* is ignored in evaluation and is removed during training. Pascal VOC [4] and COCO [12] are two common datasets for general object detection, where the number of boxes per image is around 3 boxes/image and 7 boxes/image, respectively. We do not show the results on these two datasets here but in Appendix C.1 because the number of boxes is not large, and the time cost of NMS is minor.

All the models are trained on the training set and evaluated on the test set or the validation set. Mean average precision (mAP) at IoU threshold 0.5 is used for accuracy comparison. The speed is evaluated on a workstation with Intel(R) Xeon(R) CPU E5-2620 v4 @ 2.10GHz and TITAN XP. Both the NMS and the HNMS are implemented in C++/Cuda. Pytorch and Maskrcnn-Benchmark are used as the deep learning toolkit. The time cost is calculated based on the first 100 images.

4.2 Results on Two-Stage Detector

We use Faster R-CNN [16] as the test bed to evaluate the performance on two-stage detectors. ResNet50 is used as the backbone and feature pyramid network [10] is adopted to provide multiple feature maps. The network is abbreviated as Faster-RCNN-R50-FPN.

On CARPK and CrowdHuman, the models are trained with 20 epochs while on SKU-110K, the model is trained with 80 epochs. The initial learning rate are all 0.02, and is decreased by 10x twice at 2/3 and 8/9 of the total iterations. The weight decay is 0.0001 and the momentum is 0.9. The batch size is 16 trained on 4 GPUs. During inference, we use at most P_1 proposals for NMS on each feature map and keep at most P_2 boxes after NMS. At most P_3 proposals collected from all feature maps are passed to the RoI head network. At most 1K boxes after RoI Head network are used for evaluation. On CARPK and CrowdHuman, we have $P_1, P_2, P_3 = 9K, 2K, 4K$ and on SKU-110K, it is $9K, 1K, 1K$ if these numbers are not explicitly specified. The ablation study of the parameters P_1 is also presented as follows, which plays an important role in the NMS speed and the accuracy.

Both RPN and RoI head network apply NMS to suppress the co-located boxes. For RPN, the NMS threshold is 0.7 and we also set $\alpha = 0.7$ for HNMS. The NMS in RoI head network is not altered since it is fast enough. For example in CARPK, it takes 3.3ms and 0.08% of the total time for inference.

The results are shown in Table 1. As we can see, HNMS can achieve comparable accuracy but with significant less time cost on RPN-NMS for all three datasets and on both CPU and GPU. For instance, on CARPK, we can use one IoUHash function to achieve slightly higher mAP (97.1% vs 96.9%) with 7.4x speed.

When we use more HNMS processes, the accuracy is dropped for CARPK, and increased slightly for SKU-110K and CrowdHuman. The reason is that with more filtering, HNMS could suppress more positive boxes, which leads to slight recall drop. On the other hand, it can suppress more negative boxes, which improves the precision. Another observation is that the time cost of the baseline NMS is not consistent among different datasets. The reason is that the complexity ranges from $O(N \log(N) + N)$ to $O(N \log(N) + N^2)$ and thus the time cost is data-dependent.

Varying α . Fig. 4 shows the accuracy as a function of α with different K . With a fixed K , the accuracy is normally increased first and then decreased with increasing α . The reason is that if α is too small, the hash cell will be quite large, which will suppress lots of positive boxes. if α is too large, the cell size will become tiny, which fails to suppress enough negative boxes. In the latter case, the accuracy can be improved by more HNMS (increasing K). For example in Fig. 4(c) at $\alpha = 0.8$, mAP is improved when K is increased from 1 to 4.

Varying P_1 . To reduce the time cost, one can use top fewer boxes (lower P_1) based on objectness in RPN for NMS filtering. With different numbers of boxes, we have the result illustrated in Fig. 5 with our approach denoted as HNMS- α/K , and have following observations.

Table 2: Experimental results with Retina-R50-FPN. The columns of HNMS, NMS and Total represent the time cost in ms. Speed is for the total cost relative to NMS.

(a) CARPK										
		CPU				GPU				
	K	mAP	HNMS	NMS	Speed	Total	HNMS	NMS	Speed	Total
NMS		94.8		260.9	1x	2071.1		134.7	1x	250.9
	1	95.3	23.6	194.2	1.2x	1761.9	0.9	33.1	4.0x	149.1
HNMS	2	95.3	34.0	161.7	1.3x	1762.6	1.4	18.4	6.8x	121.9
+NMS	3	95.2	46.1	140.4	1.4x	1794.6	2.5	19.5	6.1x	142.1
	4	95.2	51.4	122.4	1.5x	1732.6	3.0	14.6	7.7x	131.3

(b) SKU-110K										
		CPU				GPU				
	K	mAP	HNMS	NMS	Speed	Total	HNMS	NMS	Speed	Total
NMS		91.6		185.2	1x	1640.9		121.1	1x	217.9
	1	91.6	19.4	124.5	1.3x	1576.3	0.7	18.8	6.2x	115.8
HNMS	2	91.6	33.9	104.2	1.3x	1567.6	1.4	14.0	7.9x	111.3
+NMS	3	91.5	42.7	88.2	1.4x	1571.8	2.1	11.3	9.1x	109.0
	4	91.5	50.3	81.0	1.4x	1531.5	2.8	10.9	8.9x	111.4

1. The accuracy can be boosted significantly by simply increasing the number of boxes used for NMS. For example from 1000 to 9000, the accuracy can be improved from 95.0 to 96.9, resulting in nearly 2 points gain on CARPK. This also demonstrates the necessity of more boxes for crowded scene.
2. With the same time cost, our approach can achieve higher accuracy. For example in CPU, NMS obtains 95.4 mAP with more than 10ms, but HNMS achieves 96.4 mAP with less than 10ms, which results in 1% mAP improvement.
3. With similar accuracy, HNMS can achieve much faster speed, which is consistent with the results in Table 1.
4. In GPU, time cost of our approach is less sensitive to the number of boxes. For HNMS-0.7/1, the time cost increases from 2.4ms slightly to 2.9ms when the number of boxes is from 1000 to 9000. This is because our approach is more friendly in parallel computing.

4.3 Results on One-Stage Detector

RetinaNet [10] is used as a representative one-stage detector and Resnet50 with FPN is as the backbone. The model is short as Retina-R50-FPN. On CARPK and SKU-110K, the model is trained with 40 epochs, while on CrowdHuman, it is 20 epochs. The initial learning rate is 0.01 for CARPK, 0.005 for SKU-110K and 0.02 for CrowdHuman. The learning rate is decreased by 10x twice at 2/3 and 8/9 of the total iterations. The weight decay is 0.0001, and the momentum is 0.9. The batch size is 16 trained on 4 GPUs. For NMS, we use at most $P_1 = 9K$ boxes by default and use at most 1K final boxes for evaluation. The NMS threshold is 0.5.

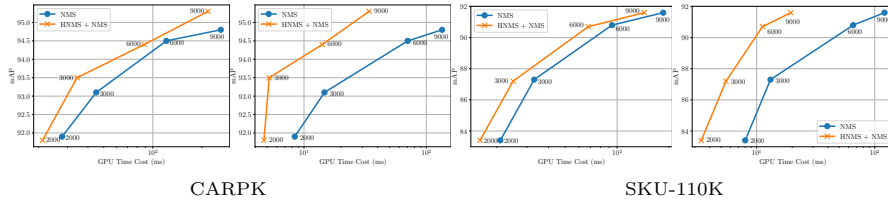


Fig. 6: Accuracy vs GPU time cost with different maximum numbers of boxes for suppression filtering in Retina-R50-FPN. HNMS is as a pre-filter before applying the NMS.

As discussed in Sec. 3.3, we use HNMS as a pre-filter before applying NMS. To reduce suppressing positive boxes, we use a higher $\alpha = 0.73$. The corresponding lower bound is 0.502, slightly higher than the NMS threshold (0.5). The results are shown in Table 2 with different K for CARPK and SKU-110K. The results on CrowdHuman can be found in Appendix C.2. When $K = 1$, the accuracy of HNMS is consistently comparable (or slightly better) with the baseline, but with higher speed on the suppression component. For example on CARPK with GPU, the speed-up is 4x (6.8x for $K = 2$) with slightly better accuracy. On SKU-110K, the speed-up is 6.2x (7.9x for $K = 2$) with the same accuracy.

When we increase K , more time is spent for pre-filtering, but fewer boxes are passed to NMS. The accuracy is penalized because more positive boxes could be removed as discussed in Sec. 3.3. For example on SKU-110K with GPU, when K changes from 1 to 4, the time cost of pre-filtering takes 0.7ms to 2.8ms. The time cost of NMS is decreased from 18.8ms to 14.0ms, and the overall speed is improved from 6.2x to around 9x. The accuracy stays the same at $K = 1, 2$, and is slightly dropped by 0.1 point at $K = 3, 4$.

Varying P_1 . Fig. 6 shows the accuracy as a function of time cost in NMS or HNMS+NMS when we vary the maximum numbers of boxes used for filtering with $K = 1$. With comparable accuracy, the time cost with HNMS as pre-filter always reduces dramatically, especially for GPU.

One alternative is to replace NMS with SoftNMS [1], and use our HNMS for pre-filtering. We leave this result in Appendix C.3.

5 Conclusion

We studied the efficiency problem of NMS in object detection and proposed a Hashing-based NMS algorithm to improve the speed. The key idea is to hash each bounding box to a discrete cell and suppress the boxes with smaller confidences within each cell. To implement this, we proposed a novel IoUHash function, which guarantees the closeness of the boxes by a lower IoU bound. Comprehensive experiments were conducted to verify the significant speed improvement with comparable accuracy.

References

1. Bodla, N., Singh, B., Chellappa, R., Davis, L.S.: Soft-nms - improving object detection with one line of code. In: IEEE International Conference on Computer Vision, ICCV 2017, Venice, Italy, October 22-29, 2017. pp. 5562–5570 (2017). <https://doi.org/10.1109/ICCV.2017.593>, <https://doi.org/10.1109/ICCV.2017.593>
2. Cai, L., Zhao, B., Wang, Z., Lin, J., Foo, C.S., Aly, M.M.S., Chandrasekhar, V.: Maxpoolnms: Getting rid of NMS bottlenecks in two-stage object detectors. In: IEEE Conference on Computer Vision and Pattern Recognition, CVPR 2019, Long Beach, CA, USA, June 16-20, 2019. pp. 9356–9364 (2019)
3. Datar, M., Immorlica, N., Indyk, P., Mirrokni, V.S.: Locality-sensitive hashing scheme based on p-stable distributions. In: Symposium on Computational Geometry. pp. 253–262 (2004)
4. Everingham, M., Eslami, S.A., Van Gool, L., Williams, C.K., Winn, J., Zisserman, A.: The pascal visual object classes challenge: A retrospective. *International Journal of Computer Vision (IJCV)* **111**(1), 98–136 (2015)
5. Goldman, E., Herzig, R., Eisenschtat, A., Goldberger, J., Hassner, T.: Precise detection in densely packed scenes. In: IEEE Conference on Computer Vision and Pattern Recognition, CVPR 2019, Long Beach, CA, USA, June 16-20, 2019. pp. 5227–5236 (2019)
6. He, Y., Zhu, C., Wang, J., Savvides, M., Zhang, X.: Bounding box regression with uncertainty for accurate object detection. In: IEEE Conference on Computer Vision and Pattern Recognition, CVPR 2019, Long Beach, CA, USA, June 16-20, 2019. pp. 2888–2897 (2019)
7. Hosang, J.H., Benenson, R., Schiele, B.: Learning non-maximum suppression. In: 2017 IEEE Conference on Computer Vision and Pattern Recognition, CVPR 2017, Honolulu, HI, USA, July 21-26, 2017. pp. 6469–6477 (2017). <https://doi.org/10.1109/CVPR.2017.685>, <https://doi.org/10.1109/CVPR.2017.685>
8. Hsieh, M., Lin, Y., Hsu, W.H.: Drone-based object counting by spatially regularized regional proposal network. In: IEEE International Conference on Computer Vision, ICCV 2017, Venice, Italy, October 22-29, 2017. pp. 4165–4173 (2017). <https://doi.org/10.1109/ICCV.2017.446>, <http://doi.ieeecomputersociety.org/10.1109/ICCV.2017.446>
9. Indyk, P., Motwani, R.: Approximate nearest neighbors: Towards removing the curse of dimensionality. In: STOC. pp. 604–613 (1998)
10. Lin, T., Dollár, P., Girshick, R.B., He, K., Hariharan, B., Belongie, S.J.: Feature pyramid networks for object detection. In: 2017 IEEE Conference on Computer Vision and Pattern Recognition, CVPR 2017, Honolulu, HI, USA, July 21-26, 2017. pp. 936–944 (2017). <https://doi.org/10.1109/CVPR.2017.106>, <https://doi.org/10.1109/CVPR.2017.106>
11. Lin, T., Goyal, P., Girshick, R.B., He, K., Dollár, P.: Focal loss for dense object detection. In: IEEE International Conference on Computer Vision, ICCV 2017, Venice, Italy, October 22-29, 2017. pp. 2999–3007. IEEE Computer Society (2017). <https://doi.org/10.1109/ICCV.2017.324>, <https://doi.org/10.1109/ICCV.2017.324>
12. Lin, T.Y., Maire, M., Belongie, S., Hays, J., Perona, P., Ramanan, D., Dollár, P., Zitnick, C.L.: Microsoft COCO: Common objects in context. In: ECCV (2014)

13. Liu, S., Lu, C., Jia, J.: Box aggregation for proposal decimation: Last mile of object detection. In: 2015 IEEE International Conference on Computer Vision, ICCV 2015, Santiago, Chile, December 7-13, 2015. pp. 2569–2577 (2015)
14. Liu, W., Anguelov, D., Erhan, D., Szegedy, C., Reed, S.E., Fu, C., Berg, A.C.: SSD: single shot multibox detector. In: Computer Vision - ECCV 2016 - 14th European Conference, Amsterdam, The Netherlands, October 11-14, 2016, Proceedings, Part I. pp. 21–37 (2016)
15. Redmon, J., Farhadi, A.: YOLO9000: better, faster, stronger. In: 2017 IEEE Conference on Computer Vision and Pattern Recognition, CVPR 2017, Honolulu, HI, USA, July 21-26, 2017. pp. 6517–6525 (2017). <https://doi.org/10.1109/CVPR.2017.690>, <https://doi.org/10.1109/CVPR.2017.690>
16. Ren, S., He, K., Girshick, R.B., Sun, J.: Faster R-CNN: towards real-time object detection with region proposal networks. *IEEE Trans. Pattern Anal. Mach. Intell.* **39**(6), 1137–1149 (2017). <https://doi.org/10.1109/TPAMI.2016.2577031>, <https://doi.org/10.1109/TPAMI.2016.2577031>
17. Shao, S., Zhao, Z., Li, B., Xiao, T., Yu, G., Zhang, X., Sun, J.: Crowdhuman: A benchmark for detecting human in a crowd. *CoRR* **abs/1805.00123** (2018), <http://arxiv.org/abs/1805.00123>
18. Wang, J., Wang, J., Song, J., Xu, X., Shen, H.T., Li, S.: Optimized cartesian k -means. *CoRR* **abs/1405.4054** (2014), <http://arxiv.org/abs/1405.4054>
19. Wang, J., Wang, J., Yu, N., Li, S.: Order preserving hashing for approximate nearest neighbor search. In: Jaimes, A., Sebe, N., Boujemaa, N., Gatica-Perez, D., Shamma, D.A., Worring, M., Zimmermann, R. (eds.) *ACM Multimedia Conference, MM '13*, Barcelona, Spain, October 21-25, 2013. pp. 133–142. *ACM* (2013). <https://doi.org/10.1145/2502081.2502100>, <https://doi.org/10.1145/2502081.2502100>
20. Wang, J., Zhang, T., Song, J., Sebe, N., Shen, H.T.: A survey on learning to hash. *IEEE Trans. Pattern Anal. Mach. Intell.* **40**(4), 769–790 (2018). <https://doi.org/10.1109/TPAMI.2017.2699960>, <https://doi.org/10.1109/TPAMI.2017.2699960>
21. Weiss, Y., Torralba, A., Fergus, R.: Spectral hashing. In: *NIPS*. pp. 1753–1760 (2008)

Appendix

A IoU Lower Bound

In Sec. 3.1 (main paper), we discussed how the IoU lower bound (given two boxes are hashed to the same cell) is calculated. Alg. 4 summarizes the details.

To derive this algorithm, we implicitly relied on the conclusions in Theorem 1 and Theorem 2. Here, we present the proof.

Theorem 1. *With Eqn. 15 and Eqn. 14 (main paper), IoU is unrelated with b_x , b_y , W_0 , H_0 , i , j , m , n , but only depends on α , i_k , j_k , m_k and n_k .*

Proof. As demonstrated in the paper, the intersection is larger than 0 since Eqn. 14 (main paper) holds. Thus, we can write the intersection as

$$I = F(r - l)F(b - t) = (r - l)(b - t), \quad (17)$$

where r , l , b , t are defined in Eqn. 10 (main paper) and Eqn. 11 (main paper), $F(x) = x$ if $x \geq 0$ and 0, otherwise. Substituting Eqn. 10 (main) and Eqn. 15 (main paper), we have

$$r - l = \min(x_1 + \frac{1}{2}w_1, x_2 + \frac{1}{2}w_2) - \max(x_1 - \frac{1}{2}w_1, x_2 - \frac{1}{2}w_2) \quad (18)$$

$$(x_k \pm \frac{1}{2}w_k) = b_x\delta_i + (m + m_1)\delta_i \pm \frac{W_0}{2\alpha^{i+i_k}} \quad (19)$$

$$= b_x\delta_i + m\delta_i + m_1\delta_i \pm \frac{W_0}{2\alpha^{i+i_k}}, k \in \{1, 2\} \quad (20)$$

The item of $(b_x\delta_i + m\delta_i)$ is unrelated with k , and thus it can be removed for Eqn. 18. With the definition of δ_i in Eqn. 4 (main paper), we have

$$r - l = \frac{W_0}{\alpha^i} F_w(i_1, i_2, m_1, m_2) \quad (21)$$

$$F_w() \triangleq \min(m_1 + \frac{1}{2\alpha^{i_1}}, m_2 + \frac{1}{2\alpha^{i_2}}) - \max(m_1 - \frac{1}{2\alpha^{i_1}}, m_2 - \frac{1}{2\alpha^{i_2}}) \quad (22)$$

where $F_w()$ is a function after we extract W_0/α^i and does not depend on W_0 and i . Similarly, we have

$$b - t = \frac{H_0}{\alpha^j} F_h(j_1, j_2, n_1, n_2). \quad (23)$$

The area of the two boxes are

$$A_k = \frac{W_0 H_0}{\alpha^{i+j+i_k+j_k}}, k \in \{1, 2\}. \quad (24)$$

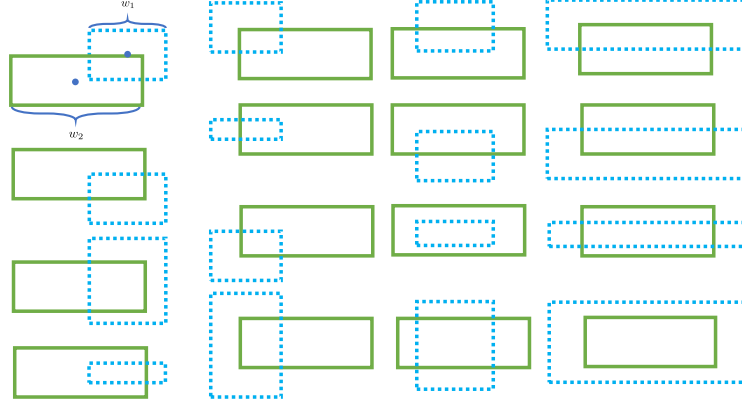


Fig. 7: Different positions between two overlapped boxes. Assume that the position of the green box is fixed, and the blue box can be floating anywhere as long as they are overlapped.

Thus, IoU can be calculated by

$$\text{IoU} = \frac{I}{A_1 + A_2 - I} = \frac{1}{\frac{A_1 + A_2}{I} - 1} \quad (25)$$

$$= \frac{1}{\frac{1/\alpha^{i_1+j_1} + 1/\alpha^{i_2+j_2}}{F_w(i_1, i_2, m_1, m_2) F_h(j_1, j_2, n_1, n_2)} - 1}, \quad (26)$$

which demonstrates that IoU has no relation with the cell index, but only depends on the offsets to the cell center.

Lemma 1. *The minimum IoU is located at the boundary of m_1 (equal to -0.5 or 0.5 since the range is from -0.5 to 0.5 as in Eqn. 15 of the main paper) given all other variables fixed.*

Proof. Since $A_k, t - b$ has no relation with m_1 , the lemma is equivalent to prove that the minimum of F_w in Eqn. 22 is located at the boundary of m_1 . The first min operation in F_w is a concave function of m_1 , and the second of negative max operation is also a concave function of m_1 . Thus, F_w is concave with m_1 , which concludes that the minimum value must be at the boundary of m_1 .

Lemma 2. *The minimum IoU is located at the boundary of i_1 (equal to -0.5 or 0.5) given all other variables fixed.*

Proof. Rather than starting from Eqn. 26, we study each position relationship between two overlapped boxes. Fig 7 enumerates all relations. The idea is to verify for each position relationship, IoU is the smallest if w_1 (parameterized by i_1) is at the boundary with all other variables fixed.

Taking the top-left one as an example, we can write the intersection as

$$I = \left(\frac{1}{2}w_1 + \frac{1}{2}w_2 - |x_1 - x_2|\right)\left(\frac{1}{2}h_1 + \frac{1}{2}h_2 - |y_1 - y_2|\right) \quad (27)$$

Algorithm 4 Lower IoU Bound for IoUHash

Input: α
Output: lower IoU bound
 1: **if** Eqn. 14 does not hold **then**
 2: return 0
 3: **end if**
 4: $\text{min_iou} = 1$
 5: $W_0, H_0, b_x, b_y = 1, 1, 0, 0$
 6: **for** each $\{i_k, j_k, m_k, n_k | k = 1, 2\}$ in $\{-0.5, 0.5\}^8$ **do**
 7: Derive $\{w_k, h_k, x_k, y_k | k = 1, 2\}$ from Eqn. 15
 8: Calculate iou
 9: **if** $\text{min_iou} > \text{iou}$ **then**
 10: $\text{min_iou} = \text{iou}$
 11: **end if**
 12: **end for**
 13: return min_iou

which is a linear function of w_1 . Since the area is also linear with w_1 , IoU is monotonous with w_1 . If it is monotonously increasing, IoU achieves the smallest if w_1 is the smallest or i_1 is equal to -0.5. If it is monotonously decreasing, we can increase i_1 or w_1 until the relationship becomes the top-right of Fig. 7, where IoU is even smaller if the width is even wider. Thus, IoU achieves the smallest when w_1 is the largest or i_1 equals 0.5. Verifying all other relations, we can conclude that i_1 should be in the boundary if IoU is the smallest.

Theorem 2. Under Eqn. 15 and Eqn. 14 in the main paper, the minimum IoU must reside in one of the boundaries, where $i_k, j_k, m_k,$ and n_k equals -0.5 or 0.5.

Proof. Assume that i_k^*, j_k^*, m_k^* and n_k^* gives the minimum IoU, and at least one of the variables is not at the boundary. Given the Lemma 1 and Lemma 2, we can conclude IoU can be lower if that variable goes to the boundary with other variables fixed. Thus, all those variables must be in the boundary if IoU is smallest.

B GPU Implementation

Sec. 3 (main paper) briefly discussed the GPU implementation. Here we present more details, as shown in Fig. 8.

The first step is to hash each box into the hash index (i, j, m, n) , and then map it to a *representative value* by

$$c(i, j, m, n) = i + j * 10^4 + m * 10^8 + n * 10^{12}. \quad (28)$$

The function can be any one as long as the code (i, j, m, n) is deterministic by the representative value, which helps to identify which boxes shares the same code.

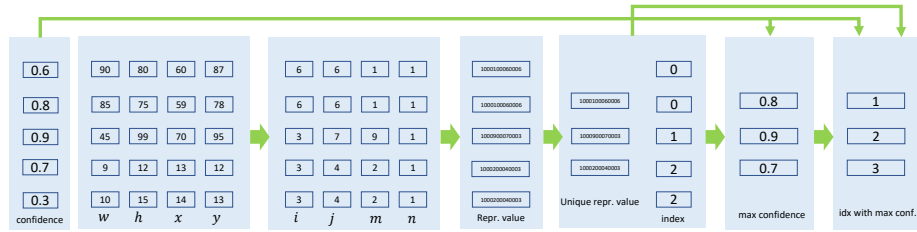


Fig. 8: Illustration of GPU Implementation. Each bounding box is first hashed to the code, which is further mapped to a representative value. Then, a unique representative code and the inverse index for each box is calculated. Third, the maximum confidence with each cell is calculated based on atomic operation of max. Last, the final index is derived based on atomic operation of compare-and-swap.

Although Eqn 28 does not satisfy the requirement theoretically, the function works in practice since the image size is normally limited (less than 2000×2000).

Next, we leverage the implementation of `torch.unique`¹ to get the unique representative codes and the reverse index of each box to the unique code.

Third, we calculate the maximum confidence value within the same hash cell. Specifically, each bounding box is scanned one by one (not the unique representative code), and an array is allocated to record the largest confidence (initialized as 0). If the box’s confidence is higher than the recorded largest confidence, then replace it. Since multiple GPU cores could modify the value at the same address, we use the atomic operation of `atomicMax`² in CUDA library to compare and replace. The function of `atomicMax` only accepts the integer input, so each floating-valued confidence score f is converted to an integer by $f \times 10^6 + 10^5$. We will discuss the usage of addition with 10^5 in the last step. Since the confidence is within 0 to 1, this conversion is enough in practice.

Last, we find the index with the maximum confidence score for each unique code. This process is implemented by scanning each bounding box based on the atomic operation of `atomicCAS`³. That is, for each bounding box, swap its index if the box’s integer-converted confidence equals the maximum one in the array. Note, after the index is swapped, the array stores the index rather than the integer-converted confidence. To make sure the index is not swapped again by other boxes, we make the integer-converted confidence at least 10^5 .

¹ <https://pytorch.org/docs/master/torch.html#torch.unique>

² <https://docs.nvidia.com/cuda/cuda-c-programming-guide/index.html#atomicmax>

³ <https://docs.nvidia.com/cuda/cuda-c-programming-guide/index.html#atomiccas>

Table 3: Experimental results on CrowdHuman with Retina-R50-FPN. The columns of HNMS, NMS and Total represent the time cost in ms. Speed is for the total cost relative to NMS.

	K	mAP	CPU				GPU			
			HNMS	NMS	Speed	Total	HNMS	NMS	Speed	Total
NMS		77.7		327.8	1x	1870.9		143.9	1x	260.5
	1	77.8	25.0	268.7	1.1x	1653.4	0.9	65.1	2.2x	182.1
HNMS	2	77.6	42.2	234.5	1.2x	1837.4	1.6	39.4	3.5x	151.3
+NMS	3	77.5	56.8	216.4	1.2x	1858.9	2.3	29.4	4.5x	139.1
	4	77.4	66.2	193.5	1.3x	1841.9	3.2	24.3	5.2x	142.2

C Experiments

C.1 VOC and COCO

Pascal VOC [4] and COCO [12] are two widely-used datasets for object detection. On average, each image has 3 boxes in VOC and 7 boxes for COCO. Since the object density is small, it is not beneficial to feed more boxes into NMS. On VOC, we trained a model of Faster-RCNN-R34-FPN with 9000 iterations and achieved consistent 77.2% mAP for P_1 ⁴ ranging from 1000 to 9000. On COCO, we trained a model of Faster-RCNN-R50-FPN with 180000 iterations and achieved consistent 37.4% mAP_{0.5:0.95} for P_1 ranging from 1000 to 9000. The accuracy on COCO is based on the average mAP over IoU threshold 0.5:0.05:0.95 as commonly adopted in this dataset, and all other accuracies are based on mAP at 0.5 as described in the main paper.

Regarding the time cost at $P_1 = 1000$ for CPU, NMS takes $5.5/1473.6 = 0.4\%$ of the total cost on VOC and $6.5/1998.5 = 0.3\%$ on COCO. For GPU, it is $2.3/47.9 = 4.8\%$ on VOC and $2.7/67.1 = 4.0\%$ on COCO. Due to the low time cost, we mainly focus on the crowded scenarios as in the main paper, e.g. in CARPK [8] with an average of 103 objects for each image.

C.2 Supplementary for Table 2

In Table 2 of the main paper, we showed results on CARPK and SKU-100K. Fig. 3 shows the results on CrowdHuman and we have similar observations: comparable accuracy but higher speed, especially for GPU.

C.3 Application on SoftNMS

One alternative to NMS is SoftNMS [1] to achieve higher accuracy. Instead of discarding the boxes, SoftNMS decreases the confidence score. Specifically, the

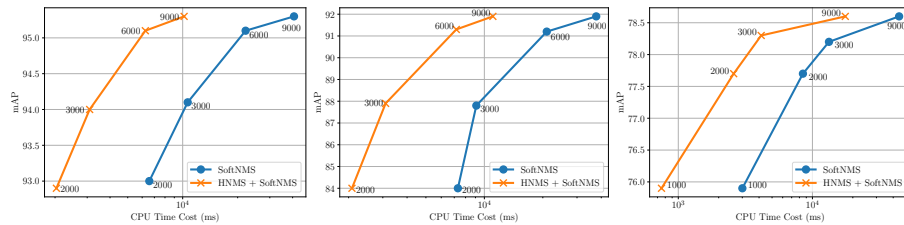
⁴ Recall that P_1 is the maximum number of boxes in each feature map (5 feature maps in total) used for NMS in RPN.

Table 4: Experiment results with Retina-R50-FPN for SoftNMS. The columns of HNMS, NMS and Total represent the CPU time cost in ms. Speed is for the total cost by HNMS and NMS.

(a) CARPK						
	K	mAP	HNMS	SoftNMS	Speed	Total
NMS		95.3		40710.5 ± 4402.8	1x	42980.8 ± 6686.9
HNMS	1	95.3	22.6 ± 5.4	10160.4 ± 2582.2	4.00x	11878.1 ± 2591.7
	2	95.4	31.8 ± 6.3	7210.5 ± 1925.8	5.62x	8901.7 ± 1939.2
	3	95.4	39.5 ± 8.1	5451.7 ± 1565.6	7.41x	7133.3 ± 1573.8
	4	95.4	49.4 ± 11.2	4701.4 ± 1372.1	8.57x	6415.1 ± 1402.6

(b) SKU-110K						
	K	mAP	HNMS	SoftNMS	Speed	Total
NMS		91.9		37673.2 ± 2564.3	1x	39260.5 ± 2692.3
HNMS	1	91.9	21.8 ± 3.5	11042.8 ± 1837.5	3.40x	12639.3 ± 1877.0
	2	92.0	30.3 ± 5.5	6902.1 ± 1144.8	5.43x	8434.5 ± 1214.3
	3	92.0	38.1 ± 6.5	5524.2 ± 943.4	6.77x	7038.9 ± 1011.7
	4	92.0	45.5 ± 7.0	4697.9 ± 899.0	7.94x	6258.0 ± 988.1

(c) CrowdHuman						
	K	mAP	HNMS	SoftNMS	Speed	Total
NMS		78.6		44272.1 ± 3350.4	1x	45821.6 ± 3418.3
HNMS	1	78.6	26.7 ± 6.8	17549.4 ± 2625.1	2.52x	19295.2 ± 2706.6
	2	78.6	39.0 ± 7.4	11474.2 ± 2039.7	3.85x	13125.2 ± 2053.0
	3	78.6	51.5 ± 8.8	9234.0 ± 1838.6	4.77x	10937.6 ± 1863.9
	4	78.6	65.7 ± 35.9	7940.9 ± 1713.3	5.53x	9717.2 ± 1791.1

Fig. 9: mAP vs Time cost with different maximum numbers of boxes for suppression filtering in Retina-R50-FPN. SoftNMS is used and HNMS ($K = 1$, $\alpha = 0.73$) is as pre-filtering.

algorithm iteratively 1) finds the box with the highest confidence and insert it to the *visited* list, 2) decrease all *un-visited* boxes' confidence based on the IoU similarity with the box just inserted to the *visited* list. Thus, the algorithm's

complexity is $O(N^2)$ (N is the number of boxes). Due to the lack of an efficient GPU implementation⁵, we mainly compare the time cost on CPU.

Table. 4 shows the experiment results with Retina-R50-FPN on the three datasets with $P_1 = 9000$ (maximum nubmer of boxes used for NMS in each feature map). As can be seen, the time cost of SoftNMS is quite large, e.g. 40.7 seconds on CARPK. By pre-filtering with the proposed HNMS, the time cost can be significantly reduced, e.g. to 10.2 seconds on CARPK ($K = 1$), with no accuracy regression. With more hashing functions (larger K), the time cost can be further reduced since more boxes are pre-filtered. One observation is that the time cost of the SoftNMS without pre-filtering is not consistent across the three datasets, because the confidence decreasing is skipped if the box has no overlap, which makes the time cost dependent on the data distribution. Compared with NMS, SoftNMS improves the accuracy by 0.5 in CARPK, 0.3 in SKU-110K and 0.9 in CrowdHuamn.

Varying P_1 . By altering different values of P_1 , we arrive at Fig. 9, which clearly shows the necessity of increasing P_1 and the significant gains with HNMS as pre-filtering.

⁵ The difficult part is that each iteration finds the box with maximum confidence, which relies on previous iteration.